Nucleation and growth of a stable phase in an Ising-type system

V. A. Shneidman, K. A. Jackson, and K. M. Beatty
Department of Materials Science and Engineering, The University of Arizona, Tucson, Arizona 85721
(Received 13 July 1998)

A system of nearest-neighbor interacting spins driven by a Glauber-type dynamics on a two-dimensional hexagonal lattice was studied as a model for a first order phase transition. The primary goal of the study was to verify the kinetic aspects of the conventional nucleation and growth description which is associated with the motion of the interface, the growth and decay of individual nuclei, and with their size distributions. The role of time-dependent nucleation was highlighted, and the overall kinetics of the phase transition were examined. By an artificial modification of the dynamics in order to exclude some of the paths in the formation or destruction of nuclei, coagulation effects were studied. The latter have only minor influence in the immediate vicinity of the binodal, but increase rapidly upon intrusion into the metastable phase. [S0163-1829(99)02305-X]

I. INTRODUCTION

It is hard to overestimate the role of Ising-type systems in the development of fundamental understanding of the nature of phase transitions. Thermodynamically, the attractive feature of such systems is that they are exactly solvable for sufficiently simple low-dimensional lattices.[1,2] In the dynamic case exact solutions are available only for one-dimensional cases.[3,4] Nevertheless, for higher dimensions dynamics of such systems can be obtained from large-scale computer simulations.[4–14] Such simulations provide an important insight into the validity of more intuitive descriptions, and enhance the understanding of a metastable state. The number of studies reflects the variety of applications, including ferromagnetic[15] or ferroelectric[11,16] particles, melt-to-crystal transitions,[13,14] etc.

A typical destruction of a metastable phase proceeds via nucleation and growth of stable-phase nuclei. Standard (''classical'') descriptions of both the nucleation[17] and the growth stages[18,19] are well established. Nonclassical pictures of nucleation were also developed in the more recent past.[20–22] In principle, examination of nucleation and growth dynamics in Ising-type systems should provide an estimation of accuracy of each type of the description, whether classical or nonclassical, and establish the limits of applicability of the overall nucleation picture.

The majority of studies agrees that the nucleation rate I follows the prediction

$$\ln I \propto -h^{1-d} - \psi(h), \tag{1}$$

where d is the dimension of a system and h is the magnetic field (which is proportional to undercooling, see below). $\psi(h)$ is expected to be a weak, logarithmic-type function of h. Simulations[7,9,12] confirm the leading term in Eq. (1), but there does not yet exist a definite conclusion about $\psi(h)$, so that either classical[9] or nonclassical[12] interpretations of the observations are invoked.

Still less is known about the specifically kinetic aspects of the description. For example, how accurate is the conventional description of the phase transformation kinetics due to Kolmogorov and Avrami,[18,19] which is routinely used to extract nucleation rates from simulation data?[11,12] Or how one can incorporate dynamic effects which can be due to internal nucleation-growth kinetics, but which also can arise due to finite sizes of the simulated system?[12]

Due to the very large time scales which are required to observe the decay of a metastable state, fundamental and technical (computational) issues of simulations are closely interwined and are often hard to resolve. In particular, at least *three* definitions of the nucleation rate can be required depending on the size of the system. The aforementioned definition based on the overall transformation kinetics is expected to be applicable for strong and moderate undercoolings. In the latter case the rate I can also be evaluated directly from the number of nucleated particles, provided data for time-dependent cluster distributions are available. This method also corresponds to the actual experimental measurements for crystal nucleation in glasses.[23] Alternatively, for a small system, i.e., the one for which at a given undercooling only one or a handful of nuclei can be observed, neither of the above methods can be applied, but the nucleation rate can be obtained from the average waiting time which is required to detect the first nucleus. Dynamic effects can play an important (and different) role in each of the methods. It would be of special interest to find a region where all three methods are applicable and can be compared.

Examination of the kinetic aspects of nucleation and growth in an Ising-type system is the primary goal of the present study. As a starting point, we wish to maximize information, both thermodynamic and kinetic, which can be extracted from simulation at equilibrium ($h=0$). At $h=0$ there are no restrictions which arise due to finite lifetime of the metastable state, and accuracy of the treatment is limited only by computational power. From the equilibrium observations one can attempt to predict the nucleation kinetics in the undercooled region, and compare those predictions with the actual simulation data. In fact, a similar situation takes place in real-life experiments as well (e.g., there are practically no systems where the interfacial energy is measured below the melting point, while accurate equilibrium measurements are often possible).

A phenomenon which cannot be predicted quantitatively from equilibrium simulations and which has to be taken into account at deeper undercoolings, is coagulation of clusters.[24,25] Here more empirical approaches are to be invoked, and Ising-type models provide a unique opportunity to isolate coagulation effects by blocking the mainstream nucleation path and comparing the restricted and nonrestricted dynamics (see next section).

The computational model which will be used is due to Jackson, Gilmer, and Tëmkin (JGT) (Ref. 13) and was originally developed to describe crystallization of an undercooled melt with a special focus on post-nucleation motion of the interface in three-dimensional, two-component systems. The present study is more nucleation oriented, and will be restricted to two-dimensional and one-component situations. A somewhat less studied, hexagonal lattice will be considered. This lattice is more symmetric than the traditional square grid, so that lattice-dependent anisotropic effects for small clusters are expected to be less pronounced. Although some exact equilibrium results are available for the hexagonal case as well,[2] the main emphasis of the study will be on ''measuring'' the key parameters, since exact solubility will not hold for any more realistic generalization.

II. THE MODEL AND CLASSICAL NUCLEATION THEORY

A. Model

In the JGT model the down spin is allowed to flip with a probability $\nu^{\mp}$ while the up spin flips with a (generally different) probability $\nu^{\pm}$. The phases associated with the predominantly up or down phases are relevant to ''solid'' and ''liquid'' in the model, although in the present study this analogy will not be pursued, except for occasional use of terminology. The transition probabilities are given by

$$\nu^{\mp} = \nu \exp\{-\Delta S\},$$

$$\nu^{\pm} = \nu \exp\{H/T\}. \tag{2}$$

Here ΔS (the ''entropy of fusion'') will be the main controlling parameter of the problem, and the energy H is determined by interaction between the nearest up spins. The energy of the up-up interaction is given by a constant ϕ per bond; note that in this description the JGT spins effectively take values 0 (down) and 1 (up).

Considering $\nu^{\mp}$ as a background frequency which does not depend on configuration, one has

$$\nu^{\pm} = \nu^{\mp} \exp(\delta H/T) \tag{3}$$

with temperature T measured in the units of Boltzmann constant, and δH given by

$$\delta H = H - \Delta S T.$$

Equilibrium is achieved at

$$T_{\mathrm{eq}} = z\phi/2\Delta S$$

with z being the number of nearest neighbors. Below T_{eq} (which should also be smaller than T_c, the critical temperature), spins have a tendency to orient themselves upwards, and the positive term

$$z\phi/2 - T\Delta S$$

is equivalent to a doubled magnetic field in conventional descriptions.

In the present study the bond energy and temperature will be fixed as $z\phi/2 = 6$ and $T = 1.5$, respectively, so that equilibrium is achieved for $\Delta S_0 = 4$. Otherwise, the value

$$\delta S = \Delta S - \Delta S_0$$

is a ''reduced undercooling.'' A metastable state is achieved for $\delta S > 0$ with all spins initially oriented down. The computational realization of the model, as well as the cluster-counting procedure are described in Ref. 14.

Occasionally, truncation of the dynamics described by Eq. (2) will be performed for selected runs. The truncation is achieved by forbidding a single spin to flip in an all-down environment. Forbidding the up flips cuts off the primary nucleation path which proceeds via formation of monomers, dimers, etc. In the post-nucleation stage (i.e., when large nuclei or a flat interface are already present in the system), this allows one to eliminate the effects of coagulation with newly formed clusters and to compare the description with a nontruncated dynamics where such effects are present. Forbidding the down flip of a single up spin is required to satisfy detailed balance, so that the underlying thermodynamics remains unchanged.

B. Classical and near-classical descriptions

The classical approach[17,26] treats nucleation as a random walk of spherical nuclei in the space of their sizes. It is described by a Fokker-Planck type equation

$$\frac{\partial f}{\partial t} = -\frac{\partial j}{\partial R}, \quad j = -DN\frac{\partial}{\partial R}\frac{f}{N}. \tag{4}$$

Here f is the cluster distribution function, j is the flux and D — the diffusion coefficient in the R space. A slightly more complicated, discrete version of Eq. (4) is often considered as a starting point for the classical description. This will be discussed in the Appendix, but leads to practically identical results for the parameters considered in the present study.

The function $N(R)$ in Eq. (4) is the (quasi)equilibrium distribution which corresponds to zero flux. It is taken as proportional to the thermodynamic probability of a fluctuation

$$N \propto \exp\{-W(R)/T\} \tag{5}$$

with $W(R)$ being the minimal work required to form a given nucleus. In the two-dimensional case one has

$$W(R) = 2\pi\sigma R - \chi T \delta S \pi R^2, \tag{6}$$

with σ being a surface tension along a line, and $\chi \approx 0.93$ the equilibrium density of up spins. (The size R is defined in such a manner that πR^2 corresponds to the total number of spins in a cluster, n). The critical radius, R_*, corresponds to the maximum of $W(R)$, and the value $W_* \equiv W(R_*)$ represents a barrier to nucleation:

$$R_* = \sigma/(\chi T \delta S), \quad W_* = \pi\sigma R_*. \tag{7}$$

Strictly speaking, the classical nucleation theory cannot predict the prefactor in Eq. (5) (Ref. 27) (and evaluation of such prefactors is a difficult problem even for stable systems[28]). Traditionally, however, this prefactor is chosen in such a manner that the distribution $N_n = N(R)/2\pi R$ has no pre-exponential factor in an equation of type (5). In other words, if the classical theory[17] is to be taken literally, one should write

$$N^{CNT}(R) = N_0 2\pi R \exp\{-W(R)/T\}, \tag{8}$$

with N_0 being the number of ''monomers'' (in our case, the total number of down spins). Later theories (e.g., Ref. 29) do include a power-law prefactor in N_n, although the value of the exponent in this prefactor is nonuniversal and, most likely depends on temperature.[30]

From simulations at the equilibrium temperature (see next section) it follows that Eq. (5) works better without any prefactors, whether classical or nonclassical. Thus, this expression will be mostly used in the present work, although from a fundamental point of view the question remains open.

The work $W(R)$ and the (quasi)equilibrium distribution determine the thermodynamics of nucleation. Kinetics are determined by the diffusion coefficient D in Eq. (4). In the model under consideration D is proportional to $\nu^{\mp}$. According to Zeldovich,[17] the diffusion coefficient can be obtained from deterministic (neglecting fluctuations) growth or decay rates of individual nuclei via the Einstein relation

$$v = -(D/T)dW/dR. \tag{9}$$

Here $v(R)$ is the deterministic rate function which for surface-limited growth of nuclei (most likely, the case below T_c) has the form

$$v(R) = \frac{R_*^2}{\tau}\left(\frac{1}{R_*} - \frac{1}{R}\right). \tag{10}$$

Here τ is defined as $(dv/dR)^{-1}$ at $R = R_*$. It is worth noting that nonclassical nucleation descriptions[31] also lead to a similar expression in systems with a nonconserved order parameter, which is the case for the Ising model considered. The universality of Eq. (10) bolsters one's confidence in the validity of the kinetic description, even if some of the thermodynamic issues are yet unresolved.

In the immediate vicinity of R_*, where the absolute values $v(R)$ are small, the deterministic Eq. (10) is violated, and fluctuational corrections are important. The width of fluctuational region can be determined as

$$\Delta_R^{-2} = -\frac{1}{2T}\frac{d^2W}{dR^2}\bigg|_* = \pi\chi\delta S, \tag{11}$$

where the asterisk indicates a value calculated at the critical size. For $\Delta_R \ll R_*$, i.e., for a high nucleation barrier, and with standard boundary conditions,[17] Eq. (4) has a steady-state solution with a size-independent flux

$$j_{\rm st} = \frac{D_* N_*}{\Delta_R\sqrt{\pi}} = \frac{\Delta_R}{2\tau\sqrt{\pi}} N_*. \tag{12}$$

The corresponding distribution function is given by

$$f_{\rm st}(R) \simeq \begin{cases} N(R), & R_* - R \gg \Delta_R, \\ \frac{1}{2}N_* \exp\{Z^2\}\,\mathrm{erfc}(Z), & |R - R_*| \ll R_*, \\ j_{\rm st}/v(R), & R - R_* \gg \Delta_R \end{cases} \tag{13}$$

with a boundary layer of width Δ_R in the vicinity of the critical size, and with $Z \equiv (R - R_*)/\Delta_R$.

The structure of the distribution given by Eq. (13) is due to the asymptotic nature of the nucleation problem, i.e., due to the conditions $W_* \gg T$ and $R_* \gg 1$. When the latter are satisfied, Eqs. (13) overlap in the common regions of applicability giving an asymptotically smooth distribution at all sizes. In the same asymptotic limit a time-dependent solution can also be obtained; the main difference at large sizes is that the steady-state flux in Eq. (13) is to be replaced by its time- (and size-) dependent value.[32,33] This solution will be described in Sec.V in connection with corresponding simulations.

The ideas of the classical description are based on what has become known as a ''droplet model,'' i.e., one which treats clusters as macroscopic drops with a negligibly thin interface and with a bulk value of the surface tension. Intuitively, the Ising-type models with nearest neighbor interaction, and below T_c, seem to be the best candidates for such a description (although a first-principle justification remains a nontrivial task[34]). Essentially nonclassical effects are expected only for long-range interactions.[10] A limitation of the literally classical description is seen only in the pre-exponential of Eq. (8). Indeed, despite the warning by Farkas,[17] it is conventionally assumed that the expressions for the (quasi)equilibrium distribution are valid down to the smallest sizes. This contradicts the asymptotic nature of the droplet model and, as one can see from the Ising-type system under consideration, the number of single up spins is determined exclusively by the parameter ΔS and has less relation to surface tension and other parameters which determine the work $W(R)$. Nevertheless, these limitations of the droplet model are of a thermodynamic nature and when applied to nucleation can be overcome by *measuring* $N(R)$ at $T = T_{\rm eq}$, as discussed in the next section. Otherwise, from a purely kinetic point, the droplet model remains very attractive, and will be shown to provide a reasonably accurate description.

III. EQUILIBRIUM PROPERTIES

A. Distribution of clusters and the surface tension

At $T = T_{\rm eq}$ the quasiequilibrium distribution $N(R)$ coincides with the steady-state distribution, and is given by

$$N_{\rm eq}(R) \propto \exp(-2\pi\sigma R/T_{\rm eq}). \tag{14}$$

This exponential decay seems to be the right choice, as shown in Fig. 1. Distributions were recorded after each 10

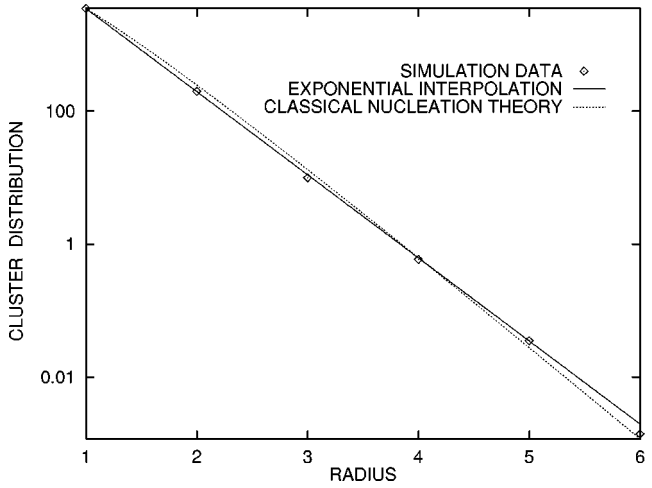

FIG. 1. Distribution of clusters on 480×480 grid at equilibrium temperature. The exponential interpolation (solid line) is used to determine the surface tension σ from Eq. (14). The classical nucleation approximation has an additional R dependence in the preexponential, Eq. (8), and is shown (for a different σ) by a dotted line.

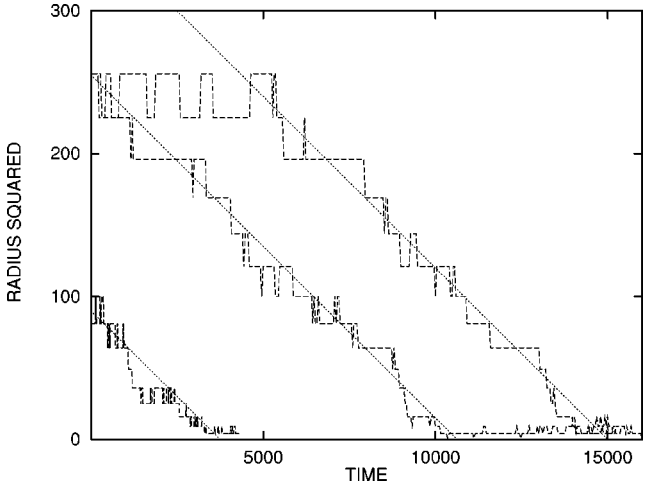

FIG. 2. Decrease of particle sizes driven by surface tension at equilibrium temperature. Simulations are shown by dashed lines. All straight dotted lines have the same slope which corresponds to $2R_*^2/\tau$ in Eq. (15). Time is the number of Monte Carlo steps.

Monte Carlo steps, with a total of 5×10^4 steps. Two runs were performed, and the final distribution is the result of the averaging.

Correspondence with simulation data for the smallest ($R=1$) and the largest ($R=6$) sizes could be coincidental (the former uncertainty due to the counting method which records the number of clusters with sizes between $R-1$ and R, the latter due to poor statistics for the largest size). Nevertheless, other points are fit well by Eq. (14), giving $\sigma=0.687$. The ''literally classical'' approximation, Eq. (8), gives a noticeably different slope, and even with an adjusted surface tension (larger by 16%) and an adjusted numerical prefactor, it gives a visually detectable curvature in Fig. 1.

B. Decay kinetics

At equilibrium Eq. (10) describes the rate of decrease of the size of a particle due to surface tension. This equation should be considered in the limit $R_*\to\infty$ while the ratio R_*^2/τ remains finite. The size of a particle with an initial value $R(0)=R_0$ is given by

$$R^2=R_0^2-2\left(\frac{R_*^2}{\tau}\right)_{\rm eq}t. \tag{15}$$

This decrease in particle size with time is shown in Fig. 2. Since the slope of the $R^2(t)$ lines is expected to be independent of R_0, it can be used to evaluate the kinetic factor R_*^2/τ. Indeed, curves obtained for different runs have approximately the same slope. Note that the initial size R_0 must be sufficiently large (9 and 16 in the examples considered) to ensure good resolution from the fluctuational clusters which at $R\lesssim3$ are abundant in the system. (The individuality of clusters is lost in way the counting method is implemented, and only their distribution is recorded, not allowing one to distinguish between a shrunk input cluster and a newly formed fluctuational cluster of the same size.)

In the next section the parameters obtained will be used in order to predict the growth or decay of individual nuclei in the undercooled region, and the motion of the interface. In subsequent sections these parameters will be used to reconstruct the nucleation kinetics.

In Ref. 8 Stauffer and Kertesz studied the transition to equilibrium distributions in an Ising model on a square grid. In principle, the kinetic parameters can be estimated from the time-dependence of such distributions.[30] However, since at least several fluctuational nuclei are required to ensure good statistics, a large grid or a large number of Monte Carlo steps is required for any appreciable R. On the other hand, the proposed method which monitors decay of artificially injected nuclei works faster for evaluation of the kinetic parameters since the required time scale is only of the order of the decay time, and the grid needs only to slightly exceed R.

IV. FLAT INTERFACE AND NUCLEI IN THE UNDERCOOLED REGION

In the undercooled region $\delta S>0$ the velocity of a flat interface $v_\infty(\delta S)$ can be obtained from Eq. (10) in the limit $R\to\infty$. The parameter R_*^2/τ in this equation which is proportional to $\nu^{\mp}$ increases slightly from its equilibrium value, being multiplied by $\exp(\delta S)$. As discussed in the Appendix, such factors must be neglected within the accuracy of the continuous approximation, but should be included in the discrete case. For the continuous case one thus has

$$v_\infty(\delta S)=\left(\frac{R_*^2}{\tau}\right)_{\rm eq}\frac{1}{R_*}=\left(\frac{R_*^2}{\tau}\right)_{\rm eq}\frac{\chi T\delta S}{\sigma}. \tag{16}$$

The corresponding discrete expression which is numerically very close is given in the Appendix as Eq. (A5).

As seen from Fig. 3, for small undercoolings, $\delta S<0.1$, the agreement of the prediction with simulation data is good (no matching parameters are used at this point). At deeper undercoolings, however, the deviation from the near-linear behavior increases. This is due to consumption of newly formed nucleated clusters by the moving interface. To isolate the effects, the truncated description was invoked where single spin flips were forbidden (see Sec. II), making nucle-

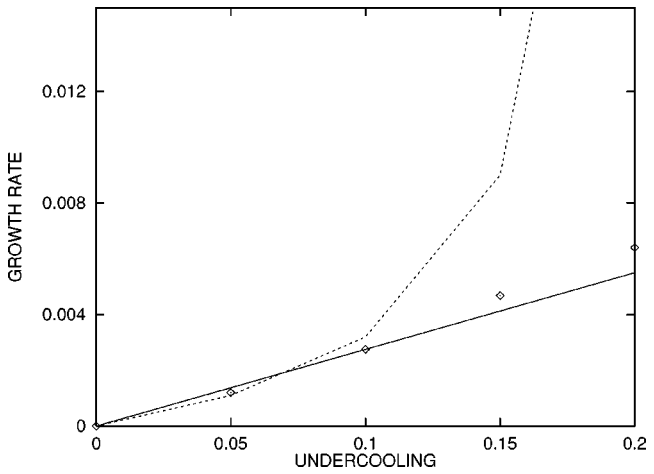

FIG. 3. Growth rate as a function of reduced undercooling δS for a flat interface. Solid line: Eq. (A5). Dotted line: simulation data for regular type spin flip dynamics. Symbols: data for truncated dynamics with some of the single spin flips forbidden (see text).

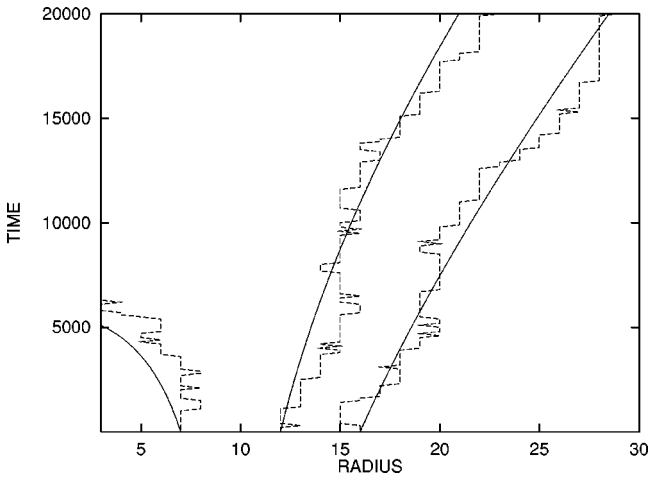

FIG. 4. Growth and decay of individual clusters with different initial sizes at a small undercooling $\delta S=0.05$. Solid lines are Eqs. (17) with $R_0=7,12,16$ (from left to right). Dashed lines: simulation results. The critical size R_* is close to 10.

ation impossible in front of the interface. As seen from Fig. 3, the truncated dynamics with no coagulation is much closer to the prediction. There is still a possibility of secondary nucleation in the bulk: up spins which are occasionally lost by the fluctuating interface can diffuse ahead of it, serving as nucleation seeds. This is observed for higher undercoolings, and most likely explains the minor differences between the corresponding symbols (diamonds) and the solid line in Fig. 3.

For a curved interface, Eq. (10) with finite R should be used in order to describe growth of overcritical and decay of subcritical clusters. This equation can be integrated, giving a family of curves parametrized by the initial size of a cluster R_0

$$\frac{t}{\tau}=\frac{R-R_0}{R_*}+\ln\frac{R-R_*}{R_0-R_*}. \tag{17}$$

Here τ can be obtained from the known value of R_*^2/τ which has a near-equilibrium value and which was obtained from Fig. 2, giving $\tau=17.48/(\delta S)^2$. Indeed, at low undercoolings predictions of Eq. (17) are in reasonable agreement with simulation data for both subcritical and overcritical values of R_0. This is seen from Fig. 4. The initial cluster was created as an up-spin island. Such islands have zero entropy and require some small time for initial equilibration which can be noted by an almost vertical initial segment in Fig. 4.

For higher undercooling coagulational corrections to growth become important, as in the case with a flat interface. Again, comparison of regular and truncated (no single spin flip) descriptions allows the effect to be highlighted. At $\delta S=0.2$ (Fig. 5) the regular and truncated descriptions differ mainly due to additional absorption of small clusters or occasional coagulation with larger particles in the regular case. Still deeper into the undercooled region, coagulation of nucleated clusters completely changes the growth dynamics, making the growth rate an explicit function of time — see Fig. 6. Here the classical (and near classical) pictures of nucleation break down for kinetic reasons, in a region where no serious modifications of thermodynamics [i.e., deviations of $W(R)$ from Eq. (6)] are expected.

V. NUCLEATION RATE AND THE DISTRIBUTION OF LARGE CLUSTERS

A. Number of nuclei

The asymptotic solution of Eq. (4) for the transient flux of nuclei in the growth region can be obtained using a matched asymptotic technique, and is given by[32,33]

$$j(R,t)=j_{\rm st}\exp\left\{-\exp\left[-\frac{t-t_i(R)}{\tau}\right]\right\}. \tag{18}$$

Here $t_i(R)$ is the ''incubation time'' and τ is defined in Sec. II. For the two-dimensional case considered, t_i is given by

$$t_i(R)=\tau\left\{\frac{R}{R_*}-2+\ln\left(\frac{R}{R_*}-1\right)+\ln\frac{2W_*}{kT}\right\}, \tag{19}$$

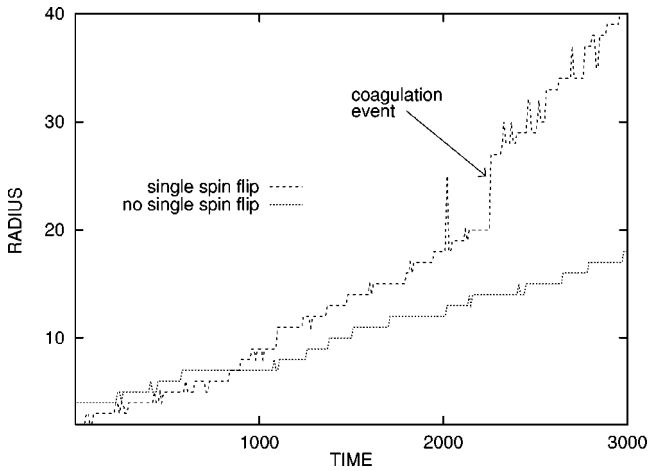

FIG. 5. Growth of overcritical particles at $\delta S=0.2$ for the regular (dashed line) and truncated (dotted line) dynamics. No single spin flip prevents the formation of new clusters, as in Fig. 3.

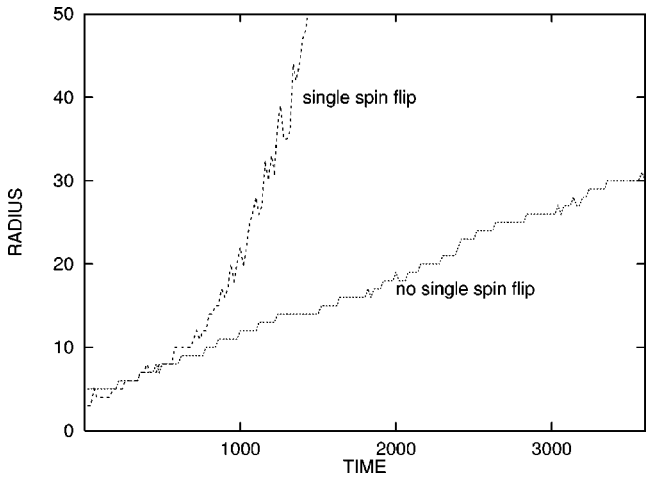

FIG. 6. Regular and truncated growth dynamics at $\delta S=0.25$. Note the absence of a linear region for the regular-type dynamics (with single spin flip).

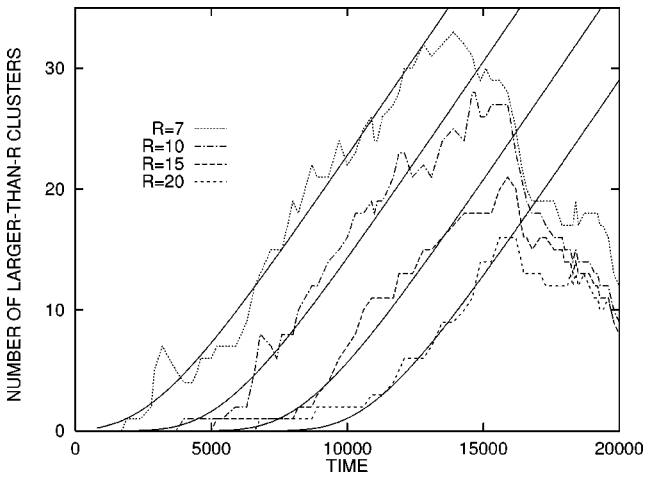

FIG. 7. Number of clusters $\rho(t)$ with size exceeding R for $\delta S=0.1$ ($R_*\approx 5$). Solid lines: Eqs. (19),(20); dashed lines; simulation data. The decrease in cluster numbers at large times is due to coagulation.

which differs by $\tau \ln 3$ from a corresponding three-dimensional expression [Eq. (12) in Ref. 33].

The number of particles with size larger than R is obtained as an integral of Eq. (18) over time, and is given by[33]

$$\rho(t)=\tau j_{\rm st}\,\mathrm{E}_1(e^{-x}), \quad x=[t-t_i(R)]/\tau. \tag{20}$$

Here E_1 is the first exponential integral.[35] In the limit $t\to\infty$ the above equation gives

$$\rho(t)\simeq j_{\rm st}(t-t_{\rm lag}), \quad t-t_{\rm lag}\gg\tau, \tag{21}$$

with $t_{\rm lag}=t_i+\gamma\tau$ ($\gamma=0.5772\cdots$ is Euler's constant) known as the ''time lag.'' Obviously, $\rho(t)$ depends on the smallest size R from which clusters are counted as ''nucleated.''

Applicability of the above equations requires many nuclei in a system, $\rho(t)\gg 1$, before the coagulation starts at $(N_0)^{-1}j_{\rm st}v^2t^3\sim 1$. With the classical estimation for the nucleation rate this gives

$$L\gg(\delta S)^{-1/6}\exp(W_*/3T) \tag{22}$$

for the size of the box, $L=\sqrt{N_0}$, with the exponential term consistent with earlier estimations.[12a] The inequality (22) implies not-too-small undercooling. At still larger undercoolings, however, particles start intensely coagulating with each other soon after the onset of nucleation, eventually making Eqs. (20), (21) inapplicable.

For the 480×480 system considered a required compromise is reached at $\delta S=0.1$. The simulated $\rho(t)$ curves are shown in Fig. 7 for different values of the counting size R together with the analytical approximation given by Eq. (20). The value of $\tau=1748$ in this equation was taken from extrapolation of equilibrium measurements (see previous section), and the value of $j_{\rm st}\approx 0.0033$ was used for all curves. The correspondence is good, and such identification of analytical and simulation results provides an accurate way of ''measuring'' the nucleation rate.

Application of the linearized Eq. (21) gives a comparable (slightly smaller) value of $j_{\rm st}$. However, since this equation requires a notably larger time scale compared to Eq. (20), it breaks down at smaller undercoolings due to onset of coagulation. On the other hand, Eq. (20) can be used at earlier times as long as the transformed area remains small, say less than 10% (and as long as $\rho(t)$ in this equation exceeds unity). In such a manner, $j_{\rm st}$ was estimated as 0.1 at $\delta S=0.15$ and as 0.2 at $\delta S=0.2$, respectively. Alternatively, if the linearized Eq. (21) was applied to the full ascending part of the $\rho(t)$ curve, the calculated values of $j_{\rm st}$ would turn out smaller, around 0.035 and 0.1, respectively. Indeed, coagulation adds clusters at small times and reduces their number on later stages, so that the slope of $\rho(t)$ curves gets smaller. The presense of coagulation effects reveals itself by the R dependence of the slope [which is not the case for a pure nucleation and growth picture — see Eq. (21)], and the above two values of $j_{\rm st}$ also should be treated as an estimation.

B. Cluster distributions

With negligible coagulation, the distribution of clusters in the growth region is given by the standard expression

$$f(R,t)=j(R,t)/v(R) \tag{23}$$

which is similar to the corresponding expression in Eq. (13), but with $j_{\rm st}$ replaced by the actual time-dependent value, Eq. (18).

In contrast to the exponentially decaying distribution below R_*, this distribution is characterized by a long, near-constant tail with a sharp cutoff. The length of the tail, $R_i(t)$, can be obtained as the inverse of Eq. (19); its maximal value is determined by the coagulation effects. For small δS a long tail with $R_i\gg R_*$ is produced via the nucleation-growth mechanism. For larger undercoolings the description is restricted to smaller times with a much shorter tail, $R_i\gtrsim R_*$, which is cutoff less abruptly, approximately as an exponential. Finally, for very large δS, the distribution is not established beyond R_* prior to the onset of coagulation, so that no independent nucleation and growth occurs.

In Fig. 8 the nucleation-growth distributions given by Eqs. (18),(19),(23) are shown at $R>2R_*$ for a small undercooling of $\delta S=0.1$. For $j_{\rm st}$ the previously mentioned measured value of 0.0033 was used, while τ was determined as

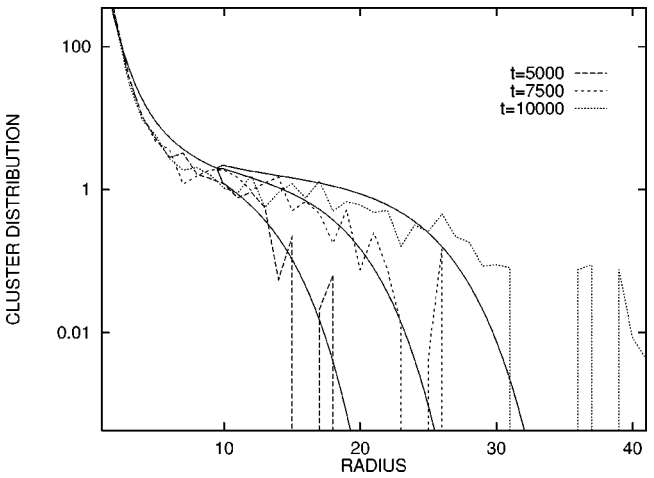

FIG. 8. Distributions of clusters at different times for $\delta S = 0.1$. Dashed and dotted lines: simulation data. Solid lines: Eqs.(13) at $R \leqslant 2R_*$ and Eqs. (23),(18) at $R > 2R_*$ with j_{st} estimated from Fig. 7. The largest clusters at $t = 10\,000$ are due to coagulation and are not described by the nucleation solution.

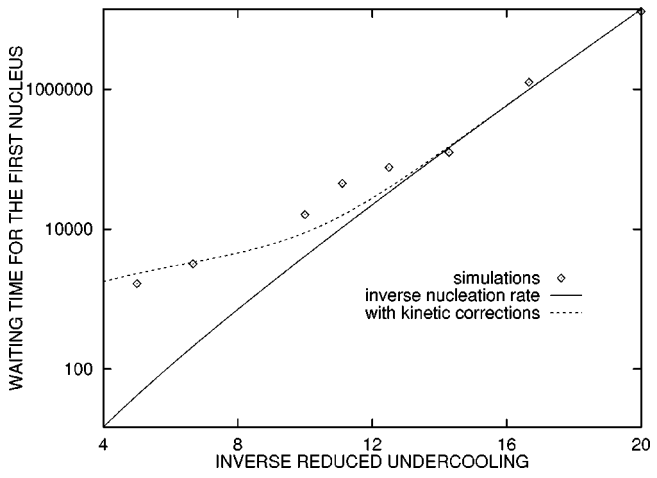

FIG. 9. Average waiting time to detect the first nucleus in a 60×60 grid as a function of δS^{-1}. Dashed line corresponds to Eqs. (19),(25). Solid line is the inverse of Eq. (12). The value at $\delta S^{-1} = 20$ is a lower estimation since not all runs resulted in nucleation.

R_* / v_∞. The results are in reasonable agreement with simulation data, except for occasional large clusters at the latest time which appear due to coagulation. For completeness of the figure, at $R < 2R_*$, the steady-state distribution is shown. The latter was obtained from Eq. (13) with a constant factor adjusted to fit the observed distribution of small clusters at $R = 2$.

The first indication of coagulation is the appearance of clusters with sizes up to $\sqrt{2}$ larger than the length of the nucleation tail due to binary collisions. This effect can be noticed even if otherwise the conditions for independent nucleation and growth are satisfied, as in Fig. 8. For larger δS coagulation affects the bulk of the cluster distribution as well. In particular, the role of the critical size becomes less pronounced. For example, at $\delta S = 0.25$ the cluster distribution will not resemble in any way (and at any time) the L shape of Fig. 8, being much closer to a power law R^{-q} with $q \approx 3$.

VI. WAITING TIME TO DETECT THE FIRST NUCLEUS

The approach of Sec. V is inapplicable to a small system where only a single nucleus can be formed. Such a nucleus will then grow to fill in the entire grid before any other particle is formed.[5,9,12] The typical nucleation time is given by $1/j_{st}$, while the growth time is of the order L/v_∞. This leads to an estimation which is opposite to the one in Eq. (22) and which defines a ''small'' system.

In a small system nucleation becomes random. Mapping to the previous description is achieved if j is treated not as a nucleation flux, but rather as probability flux (an idea due to Kolmogorov[18]). The probability density to detect a single nucleus after a waiting time t is thus given by

$$w(t) = j \exp(-\rho), \tag{24}$$

with $\rho(t)$ still given by $\int j dt$ which now can be both smaller or larger than 1.

In a steady-state case with the time-lag effects neglected, Eq. (24) is just a Poissonian distribution with the average $\bar{t} = 1/j_{st}$. Otherwise, if one assumes the validity of the large time approximation, Eq. (21), then the average waiting time is given by an expression

$$\bar{t} \approx 1/j_{st} + t_{lag}, \tag{25}$$

which is well known in connection with experimental works, e.g., Ref. 36, and where now a properly evaluated size-dependent time-lag is employed. Note that the two contributions to $\bar{t}$ in Eq. (25) are separable since j_{st} is proportional to N_0 (the system size) while t_{lag} is independent of N_0.

In the simulations, $\bar{t}$ was obtained as an average over 10 runs, of the time to detect the first nucleus of a given size R. A smaller 60×60 grid was used in order to increase $\bar{t}$ compared to t_{lag}. The value of $R = 10$ was taken as a primary choice, but values of $R = 7,12,15$ were also considered.

The simulation results are shown in Fig. 9 together with the conventional prediction, $1/j_{st}$ (an almost straight solid line). The temperature dependence of j_{st} was obtained from Eq. (12). Equation (25) is also shown (dashed line) with $R = 10$ chosen to compute the time-lag (other values of R lead to an expected minor spread in the values of $\bar{t}$). Kinetic corrections, indeed, become pronounced at larger values of the nucleation rate and substantially improve the correspondence with observations.

At $\delta S = 0.1$ the time-lag corrections are minor, and the simulated waiting time is in reasonable agreement with the inverse of the nucleation rate obtained from Fig. 7. An unexplained, not too smooth δS dependence of $\bar{t}$ should be noted. Most likely, this reflects geometrical effects due to (nonmonotonic) deviations of the excess free energies from Eq. (6), but also can be partly due to not very good statistics.

It is worth noting, that in many studies[9,12] the time to achieve a given value of the transformed area X (and not a given size R) is considered. As long as as multiple drop formation can be neglected, Eq. (25) will remain valid for such definitions provided the size R in $t_{lag}(R)$ is replaced by $L\sqrt{X/\pi}$.

VII. TRANSFORMED VOLUME FRACTION

The two-dimensional version of the Kolmogorov-Avrami (KA) expression is given by

$$X(t)=1-\exp\left(-\frac{\pi}{3N_0}j_{\rm st}v_\infty^2 t^3\right), \tag{26}$$

with $X(t)$ being the relative area covered by the new phase. This expression accounts for interaction between clusters, allowing their overlap, and assuming that otherwise the growth rate is unchanged. In the Ising-type model considered, sharp corners created by overlapping clusters facilitate flipping of near-by spins, which affects the growth. Nevertheless, one can expect that those effects are not crucial, and being the only model which accounts for arbitrary strong interactions, the KA picture can be useful for evaluation of $j_{\rm st}$ at large undercoolings.

Since the KA expression assumes a size-independent growth rate, $v=v_\infty$, it also cannot account for related transient nucleation effects[37] and for the contribution of near-critical clusters. The neglect of these two effects can be rigorously justified for a high nucleation barrier. For smaller, but still large barriers, transient nucleation effects can be included if t in Eq. (26) is replaced in accordance with[37]

$$t\to t-\tau\ln\left\{\frac{t}{\tau}\frac{W_*}{T}\right\}. \tag{27}$$

The contribution of near-critical particles can be approximately accounted for by assuming nucleation of particles with an initial size R_*, while subsequent growth is still treated as size independent.[19] Formally, this is equivalent to replacing t in Eq. (26) in accordance with

$$t\to t+\tau. \tag{28}$$

Obviously, this is not a rigorous approach since particles do not start growing right from R_*, and the neglect of contributions of smaller clusters which outnumber the critical ones is also unclear. Nevertheless, the above procedure turns out to be useful when describing the simulation data in strongly undercooled systems, before the contributions of small clusters become so large that other effects are blurred.

An important point is that the two effects, Eqs. (27) and (28) act in opposite directions. Thus, in the region of intermediate undercoolings these two effects partly compensate each other, and one can expect that the standard KA expression, Eq. (26), often works beyond the region of its formal applicability.

From Fig. 10 it can be seen that the standard KA expression works reasonably well for a moderate undercooling of $\delta S=0.1$. The nucleation rate agrees with the values obtained from Fig. 7, as will be discussed in the next section. Adding any of the aforementioned corrections worsens the correspondence. For larger δS the contribution of small clusters increases and the correction (28) is to be included in order to approximate the simulated shape. Nucleation rates are extracted from the modified KA curves by using the extrapolated, rather than the actual growth rate v_∞ (i.e., solid line from Fig. 3). This choice looks consistent since the increase in v_∞, dashed line in Fig. 3, is due to coagulation which is already taken into account in the KA interaction model.

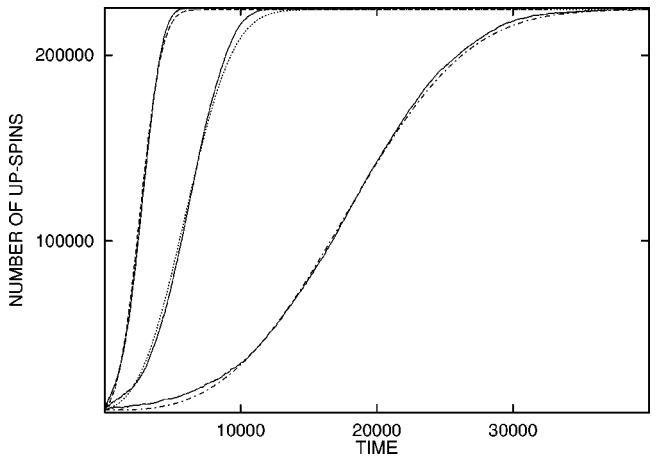

FIG. 10. Time dependence of the total number of up spins on a 480×480 grid for different values of undercooling, $\delta S=0.1$ (right), $\delta S=0.15$ (middle), and $\delta S=0.2$ (left). Solid lines: simulation data. Dashed-dotted line: the original Avrami expression, Eq. (26) for $\delta S=0.1$. Dotted and dashed lines: Eq. (26) with a shifted time, Eq. (28) for $\delta S=0.15$ and $\delta S=0.2$, respectively.

VIII. DISCUSSION

The nucleation description which is based on the ideas of droplet theory is asymptotic in nature, implying large values of the reduced nucleation barrier, W_*/T, and of the critical radius R_*. The corresponding nucleation rate is exponentially small, but the system is expected to be large enough to enable formation of many nuclei before it gets covered by the new phase. In this approximation such aspects as prefactors in the expression for the nucleation rate become of secondary importance. The dependence of those prefactors on the undercooling (magnetic field), is negligible compared to that of the exponential term, $\exp(-W_*/T)$. The principal difference between various nucleation theories is thus reduced to the manner in which the work to form a critical nucleus (sic., interfacial energy, σ) is defined. The classical approach assumed macroscopic (bulk) values of σ. Other approaches (see, e.g., Ref. 22, and references therein), include mesoscopic corrections to W_*.

It is a rare situation that all requirements of the nucleation description can be satisfied in simulations. Due to smaller values of W_*/T, nonasymptotic corrections become more important here, and the time interval for pure nucleation and growth is shortened by coagulation. In particular, transient nucleation effects are to be included in the description even if evaluation of $j_{\rm st}$, the steady-state nucleation rate, is the primary goal of a study. These effects and hence the methods employed for analysis will be very different depending on the size of the system.

In a *small* system the nucleation rate is obtained from $\bar{t}$, the average time to detect the first nucleus. In a strict asymptotic limit $j_{\rm st}$ is just an inverse of $\bar{t}$. For smaller barriers (larger undercoolings) kinetic corrections become important. In the case where $\bar{t}$ is still larger than the time-lag due to transient nucleation and growth, one can obtain $j_{\rm st}$ as

$$j_{\rm st}\simeq(\bar{t}-t_{\rm lag})^{-1}. \tag{29}$$

Otherwise, the general probability distribution for the

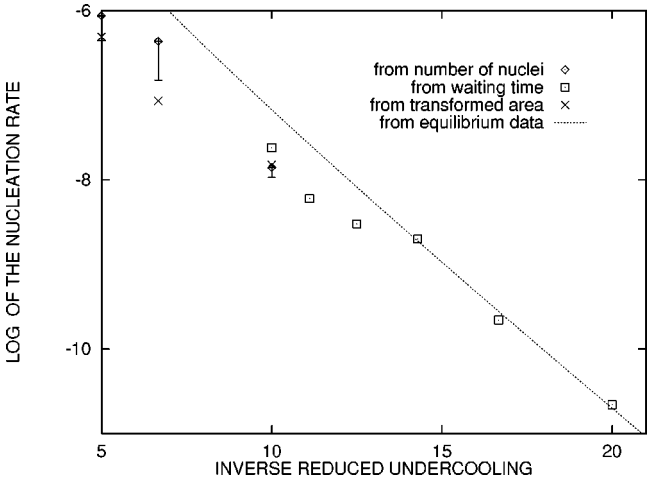

FIG. 11. Nucleation rate per spin j_{st}/N_0 obtained by different methods. Diamonds: from numbers of nucleated particles, Eq. (20), as in Fig. 7 [errorbars are obtained by using the linearized Eq. (21)]; squares: from the average waiting time corrected by the time-lag, Eq. (29); crosses: from Avrami-type expressions, as in Fig. 10.

waiting times, Eq. (24), can be used. An artificial reduction of the system size (as going from the 480×480 to 60×60 grid) can be useful to increase $\bar{t}$ compared to t_{lag} which is grid-size independent, but has its limitations due to potential contribution of boundary nucleation.[38,39] In the present study the waiting time approach permitted the examination of the region $0.05\leqslant\delta S\leqslant0.1$ — see Fig. 11.

For an *intermediate* system (larger δS) one can directly evaluate j_{st} from the observed number of nuclei $\rho(t)$ by applying Eq. (20), as in Fig. 7. Results of this approach are shown in Fig. 11 by diamonds. With increased undercooling the near-linear interval in the $\rho(t)$ dependence which represents steady-state nucleation (see Fig. 7) shortens due to coagulation between clusters. Here consideration of transient nucleation effects becomes especially helpful since they allow one to go to smaller times when coagulation is still unimportant. In the study, data for the transformed area less than 10% were used in order to evaluate j_{st}. The values of τ in Eq. (20) were taken from near-equilibrium kinetics $\tau\propto(\delta S)^{-2}$ (see Sec. IV). For larger δS, however, the validity of this extrapolation is unclear, and corresponding data in Fig. 11 for $\delta S=0.15$ and 0.2 should be treated as estimations. Rather different values of j_{st} for these undercoolings (errorbars in Fig. 11) are obtained by using the straight line approximation for $\rho(t)$ given by Eq. (21).

The Kolmogorov-Avrami (KA) type description seems to represent the only way to account for strong interactions between clusters due to their overlap, and thus to study systems with nonsmall transformed areas. At $\delta S=0.1$ a straightforward application of the KA expression gives a value of j_{st} which is consistent with direct nucleation measurements, see Fig. 11. For higher δS a minor adjustment (shift of time) in the KA expression is usually sufficient in order to fit the data (Fig. 10), although Fig. 11 suggests that agreement with nucleation rates obtained from the number of nuclei is not as good. Note that the extrapolated rather than the physical growth rates are to be used in the KA expression. The latter are enhanced by coagulation effects, but such effects are already taken into account when the KA interaction model is employed.

An interesting point is that the steady-state nucleation rate j_{st} still can have a meaning at large undercoolings when the steady-state nucleation regime is absent. In that case j_{st} is the rate of nucleation of hypothetical, non-overlapping clusters, and this definition is consistent with extrapolations of more conventional data from lower δS. Otherwise, j_{st} should be treated merely as a coefficient in the expression for the number of particles at small time, Eq. (20), or as a factor in the exponent of the KA expression at larger times.

It was shown that a detailed thermodynamic and kinetic study of clusters at equilibrium temperature (zero magnetic field) allows one to predict the nucleation behavior in the metastable region at small undercoolings. Surprisingly, the most straightforward exponential approximation of the equilibrium distribution function also turns the most accurate (see Fig. 1). This contrasts with the classical and many near-classical descriptions which have additional power-law factors in the pre-exponential. In the undercooled region the predictive abilities are limited, however, to small δS — see the dotted line in Fig. 11. At larger undercoolings the nucleation rate increases slower than the equilibrium prediction. At present, the reason for this is unclear. This could be either a single-nucleus thermodynamic effect (e.g., small nuclei start ''feeling'' the hexagonal structure of the grid), or an effect due to cluster-cluster interactions. The aforementioned pre-exponential factor could also be important, although it is not suggested by Fig. 1.

Coagulation effects cannot be predicted quantitatively from equilibrium measurements, but they are clearly observed visually, and reveal their presence by producing clusters which are too large for pure nucleation-growth mechanisms — see Fig. 8. Coagulation effects increase growth rates for flat and curved interfaces; the latter becomes obvious once those effects are ''switched off,'' as in Figs. 5 and 6. A quantitative analytical description of such effects remains, however, a task for future studies.

IX. CONCLUSION

In the present study nucleation and growth kinetics in an Ising-type system on a hexagonal grid have been analyzed. Three different methods were employed to extract the values of the nucleation rate from simulation data for, respectively, small, intermediate, and large undercoolings (magnetic fields) and were compared to each other in overlapping regions. Transient nucleation and growth effects become important with increased undercooling, but otherwise the droplet-model based nucleation picture remains consistent, especially its kinetic part. Up to moderate undercoolings the nucleation-growth behavior can be predicted quantitatively from thermodynamic and kinetic equilibrium ''measurements.''

At larger undercoolings deviations from the droplet-model predictions were observed (smaller nucleation rates), even though the critical cluster still contained several tens of spins. Coagulation effects also become important, and they can be highlighted by an artificial modification of the spin flip kinetics on the postnucleation stage.

APPENDIX: DISCRETE VERSION OF THE NUCLEATION EQUATION

The original model which was discussed by Farkas, Becker and Döring (BD) (Ref. 17) was formulated in terms of a discrete variable $n=\pi R^2$, the number of monomers in a cluster. The kinetic equation for the distribution function, $f_n=f(R)dR/dn$, has the form

$$\frac{\partial}{\partial t}f_n^{\mathrm{BD}}=j_n-j_{n+1},\quad j_n=\beta_{n-1}N_{n-1}\left(\frac{f_{n-1}}{N_{n-1}}-\frac{f_n}{N_n}\right). \tag{A1}$$

Here $\beta_n\approx D(R)(dn/dR)^2$ is the gain coefficient and the equilibrium distribution N_n is given by $N_0\exp\{-W(R)/T\}$, in accord with Eq. (8).

In the leading asymptotic approximation (large W_*/T) the BD equation gives a steady-state nucleation rate which is identical to Eq. (12), and a distribution which coincides with Eq. (13) except for a different $v(R)$, as discussed below. The functional form of the time-dependent nucleation flux, Eq. (18), also remains unchanged.[32,33] A modification is required only for the growth rate. In the general case for a smooth β_n, the discrete version of Eq. (9) takes the form[32,40]

$$v_n\simeq\beta_n\{1-\exp(W_n'/T)\}, \tag{A2}$$

where the prime indicates the derivative with respect to n, and $v_n=v(R)dn/dR$. After specification of the parameters, one obtains

$$v^{\mathrm{BD}}(R)=\frac{R_*}{\tau\chi\delta S}\{1-\exp[\chi\delta S(R_*/R-1)]\}, \tag{A3}$$

where the superscript indicates the ''Becker-Döring'' model. For small $\chi\delta S$ this expression coincides with Eq. (10). Consistency of the treatment thus requires neglecting all terms which are higher order in δS when employing the continuous description based on Eq. (4).

Modification of the growth rate leads to the following changes in the results discussed in the main part of the paper.

At equilibrium, Eq. (A3) gives

$$v^{\mathrm{BD}}=\left(\frac{R_*^2}{\tau}\right)_{\mathrm{eq}}\frac{T}{\sigma}\left\{1-\exp\left(-\frac{\sigma}{TR}\right)\right\}. \tag{A4}$$

In contrast to its continuous counterpart this expression cannot be integrated in elementary functions. In the present case this is hardly required, however, since for the values of $\sigma/T<0.5$ and the minimal value of $R>3$, the difference is unobservable within the accuracy of simulations.

For the velocity of a flat interface one has

$$v_\infty^{\mathrm{BD}}(\delta S)\simeq\left(\frac{R_*^2}{\tau}\right)_{\mathrm{eq}}\frac{T}{\sigma}[\exp(\delta S)-1]. \tag{A5}$$

Strictly speaking, the term -1 in the square brackets should be replaced by $\exp\{(\chi-1)\delta S\}$, but the difference is undetectable. Equation (A5) which numerically is very close to Eq. (16), was used for comparison with simulation data in Fig. 3.

The functional form of Eq. (20) for the number of nucleated particles also holds in the BD case. Modification of the growth rate somewhat complicates the incubation time, t_i and thus the time-lag.[33] The main difference comes from large sizes; replacing the term $\tau R/R_*$ in Eq. (19) by $R/v^{\mathrm{BD}}(\infty)$ makes this expression approximately applicable for the BD case as well. A focused study of the differences between the discrete and continuous descriptions in the time-lag problem is contained, e.g., in Ref. 41.

[1] L. Onsager, Phys. Rev. **65**, 117 (1944).

[2] R.J. Baxter, *Exactly Solved Models in Statistical Mechanics* (Academic, New York, 1982).

[3] R.J. Glauber, J. Math. Phys. **4**, 294 (1963).

[4] K. Kawasaki, in *Phase Transitions and Critical Phenomena*, edited by C. Domb and M.S. Green (Academic, New York, 1972), Vol. 2, pp. 443–501.

[5] *Applications of the Monte Carlo Method in Statistical Physics*, 2nd ed. edited by K. Binder (Springer-Verlag, New York, 1987).

[6] J. Marro, J.L. Lebowitz, and M.H. Kalos, Phys. Rev. Lett. **43**, 282 (1979).

[7] D. Stauffer, A. Coniglio, and D.W. Heermann, Phys. Rev. Lett. **49**, 1299 (1982).

[8] D. Stauffer and J. Kertesz, Physica A **177**, 381 (1991).

[9] D. Stauffer, Int. J. Mod. Phys. C **3**, 1059 (1992); Physica A **244**, 344 (1997).

[10] D.W. Heerman and W. Klein, Phys. Rev. B **27**, 1732 (1983); Phys. Rev. Lett. **50**, 1062 (1983).

[11] H.M. Duiker and P.D. Beale, Phys. Rev. B **41**, 490 (1990).

[12] (a) P.A. Rikvold, H. Tomita, S. Miyashita, and S.W. Sides, Phys. Rev. E **49**, 5080 (1994); (b) J. Lee, M.A. Novotny, and P.A. Rikvold, *ibid.* **52**, 356 (1995); (c) R.A. Ramos, P. A. Rikvold, and M. A. Novotny (unpublished).

[13] G.H. Gilmer, Mater. Sci. Eng. **65**, 15 (1984); K.A. Jackson, G.H. Gilmer, and D.E. Tëmkin, Phys. Rev. Lett. **75**, 2530 (1995); K.A. Jackson, G.H. Gilmer, D.E. Temkin, and K.M. Beatty, J. Cryst. Growth **163**, 461 (1996); K.M. Beatty and K.A. Jackson, *ibid.* **174**, 28 (1997).

[14] K.M. Beatty, Ph.D. dissertation, University of Arizona, 1997.

[15] H.L. Richards, S.W. Sides, M.A. Novotny, and P.A. Rikvold, J. Magn. Magn. Mater. **150**, 37 (1995); S.T. Chui, J. Appl. Phys. **79**, 4951 (1996); M. Kolesik, H.L. Richards, M.A. Novotny, P.A. Rikvold, and P.A. Lindgard, *ibid.* **81**, 5600 (1997); X. Kou, M.A. Novotny, and P.A. Rikvold, IEEE Trans. Magn. (to be published).

[16] H.M. Duiker, P.D. Beale, J.F. Scott, C.A. Paz de Araujo, B.M. Melnick, J.D. Cuchiaro, and L.D. McMillan, J. Appl. Phys. **68**, 5783 (1990).

[17] M. Volmer and A. Weber, Z. Phys. Chem. (Leipzig) **119**, 227 (1926); L. Farkas, *ibid.* **125**, 236 (1927); R. Becker and W. Döring, Ann. Phys. (Leipzig) **24**, 719 (1935); Ya.B. Zeldovich, Acta Physicochim. USSR **18**, 1 (1943); J. Frenkel, *Kinetic Theory of Liquids* (Oxford University Press, Oxford, 1946).

[18] A.N. Kolmogorov, Bull. Acad. Sci. USSR, Sci. Mater. Nat. **3**, 355 (1937).

[19] M. Avrami, J. Chem. Phys. **7**, 1103 (1939).
[20] J.S. Langer, Ann. Phys. (N.Y.) **54**, 258 (1969).
[21] D.W. Oxtoby and P.R. Harrowell, J. Chem. Phys. **96**, 3834 (1992).
[22] Yu.C. Shen and D.W. Oxtoby, J. Chem. Phys. **104**, 4233 (1996).
[23] P. James, Phys. Chem. Glasses **15**, 95 (1974); V. Fokin, A. Kalinina, and V. Filipovich, Fiz. Khim. Stekla **3**, 122 (1977).
[24] K. Binder and H. Müller-Krumbhaar, Phys. Rev. B **9**, 2328 (1974); K. Binder and D. Stauffer, Adv. Phys. **25**, 343 (1976); K. Binder, Phys. Rev. B **15**, 4425 (1977).
[25] P.G. van Dongen and M.H. Ernst, J. Stat. Phys. **37**, 301 (1984).
[26] F.F. Abraham, *Homogeneous Nucleation Theory* (Academic, New York, 1974).
[27] E.M. Lifshits and L.P. Pitaevskii, *Physical Kinetics* (Pergamon, New York, 1981), Sec. 99.
[28] G. Ruppeiner, Rev. Mod. Phys. **67**, 605 (1995).
[29] M.E. Fisher, Physics (Long Island City, NY) **3**, 255 (1967).
[30] V.A. Shneidman, Physica A **190**, 145 (1992).
[31] S.M. Allen and J.W. Cahn, Acta Metall. **27**, 1085 (1979).
[32] V.A. Shneidman, Sov. Phys. Tech. Phys. **32**, 76 (1987).
[33] V.A. Shneidman, Sov. Phys. Tech. Phys. **33**, 1338 (1988).
[34] J.P. Marchand and P.A. Martin, Physica A **127**, 681 (1984).
[35] M. Abramowitz and I. Stegun, *Handbook of Mathematical Functions* (Dover, New York, 1972).
[36] I. Gutzow, Contemp. Phys. **21**, 121 (1980); **21**, 243 (1980).
[37] V.A. Shneidman and M.C. Weinberg, J. Non-Cryst. Solids **160**, 89 (1993).
[38] H.L. Richards, M. Kolesik, P.-A. Lindgard, P.A. Rikvold, and M.A. Novotny, Phys. Rev. B **55**, 11 521 (1997).
[39] E.N. Cirillo and J.L. Lebowitz, J. Stat. Phys. **90**, 211 (1998).
[40] V.A. Shneidman, Phys. Lett. A **143**, 245 (1990).
[41] V.A. Shneidman and M.C. Weinberg, J. Chem. Phys. **97**, 3621 (1992).